energies

MDPI

Article

Feedstock-Dependent Phosphate Recovery in a Pilot-Scale Hydrothermal Liquefaction Bio-Crude Production

Ekaterina Ovsyannikova *, Andrea Kruse and Gero C. Becker *

Department of Conversion Technologies of Biobased Resources, Institute of Agricultural Engineering, University of Hohenheim, 70599 Stuttgart, Germany; andrea_kruse@uni-hohenheim.de

* Correspondence: e.ovsyannikova@uni-hohenheim.de (E.O.); gero.becker@uni-hohenheim.de (G.C.B.); Tel.: +49-711-459-23413 (E.O.); +49-711-459-24785 (G.C.B.)

Received: 3 December 2019; Accepted: 11 January 2020; Published: 13 January 2020

Abstract: Microalgae (*Spirulina*) and primary sewage sludge are considerable feedstocks for future fuel-producing biorefinery. These feedstocks have either a high fuel production potential (algae) or a particularly high appearance as waste (sludge). Both feedstocks bring high loads of nutrients (P, N) that must be addressed in sound biorefinery concepts that primarily target specific hydrocarbons, such as liquid fuels. Hydrothermal liquefaction (HTL), which produces bio-crude oil that is ready for catalytic upgrading (e.g., for jet fuel), is a useful starting point for such an approach. As technology advances from small-scale batches to pilot-scale continuous operations, the aspect of nutrient recovery must be reconsidered. This research presents a full analysis of relevant nutrient flows between the product phases of HTL for the two aforementioned feedstocks on the basis of pilot-scale data. From a partial experimentally derived mass balance, initial strategies for recovering the most relevant nutrients (P, N) were developed and proofed in laboratory-scale. The experimental and theoretical data from the pilot and laboratory scales are combined to present the proof of concept and provide the first mass balances of an HTL-based biorefinery modular operation for producing fertilizer (struvite) as a value-added product.

Keywords: struvite; HTL; biorefinery; renewable fuel; HyFlexFuel

1. Introduction

Hydrothermal liquefaction (HTL) of biomass presents a promising procedure [1,2] for overcoming dependency on fossil fuels and advancing toward sustainable decarburization of the transportation sector. Hydrothermal liquefaction enables the conversion of wet biomass or waste materials into bio-crude oil by using hot-compressed water (287–375 °C) [3,4] that refines downstream to liquid fuel [5]. It is of special interest in jet fuel. In biorefinery, sustainability has an important role in achieving the viability of a large-scale bio-crude facility. Nutrient recovery presents an attractive option for improving sustainability and adding value to the production chain. After HTL, the macro (P, K, N) and micro (S, Mg, Ca, Fe) nutrients that might be recovered for biomass production systems are distributed between its products, which include the HTL oil (also known as bio-crude), liquid, and solid phases. This distribution of nutrients among HTL phases depends on not only process conditions but also the nature and composition of the biomass feedstocks [6]. Furthermore, it presupposes variations in nutrient recovery strategies among various biomass feedstocks.

Significant research on HTL, and by association, nutrient recovery, has been performed in small-scale batch systems and mainly utilized algae as feedstock [7–9]. The next step toward the commercialization of biofuel production, which involves an HTL pilot-scale plant that operates in a

continuous mode, has received considerably less attention [10]. Only a few published reports relate to nutrient recovery following bio-crude production via continuous HTL. One study by Edmundson et al. [11] has demonstrated that soluble phosphate, which was recovered through acid extraction from the HTL solid phase that originated from continuous HTL of algae feedstock (total volume of system ~1.6 L), could be recycled for algae production. However, replacing nitrogen in a growth medium by using the HTL liquid phase can have a negative effect on the growth rate of algae [11]. McGinn's study [12] has considered the HTL liquid phase that results from continuous HTL of algae (total volume of system ~0.45 L). He has noted that the complete decoupling of phosphate (via struvite $MgNH_4PO_4{\cdot}6H_2O$ precipitation) and nitrogen as ammonia (through ammonia stripping) from the HTL liquid phase suggests a flexible method of recycling them for algae cultivation. To the author's knowledge, no study has previously reported on the feedstock-related fate of nutrients in a pilot-scale HTL unit or discussed nutrient recovery in a large-scale HTL scenario in relation to the distribution of nutrients. This study provides such data, which were gathered in the framework of the HyFlexFuel project. It assesses two campaigns of a continuous HTL pilot plant. Each campaign used a different feedstock—primary sewage sludge (PSS) and the microalgae *Spirulina* (*SPR*)—both of which are highly relevant to nutrient recovery.

Interest in converting sewage sludge to bio-crude via HTL has increased in the past few years [13–15] because of its availability in large volumes as the main byproduct of wastewater treatment plants, its high water content, and its embedded energy potential. In addition, it is an attractive secondary phosphate source [16]. Previous studies have found the phosphate from sewage sludge primarily in the HTL solid phase as a result of a substantial content of metal ions, such as calcium, iron, and aluminum, and the low solubility of their phosphate salts [6]. While some studies have focused on the immobilization of heavy metals from sewage sludge in the HTL solid phase [17,18], no publication has been found that targets the study of phosphate recovery from HTL solid residue of sewage sludge. Phosphate recovery from the HTL solid phase may be possible in the form of struvite ($MgNH_4PO_4{\cdot}6H_2O$), as previously demonstrated for the related process of hydrothermal carbonization (HTC). Becker et al. [19] have successfully performed phosphate and nitrogen recovery based on HTC of digested sewage sludge via precipitation of struvite from a mixture of the HTC liquid phase and acid leachate from hydrochar. Other studies have also revealed the potential of struvite production on the basis of hydrothermal treatment of various kinds of biomass [20–22]. Bauer et al. [23] have evaluated a possible approach to HTL liquid phase management by way of struvite precipitation for a wide range of biomass that includes pre-digested and digested sludge. Moreover, they have suggested that struvite precipitation from the HTL liquid phase may be economically appealing.

Microalgae are another promising feedstock for HTL. Their advantages include high annual biomass productivity, an ability to grow in poor-quality water, high water, and energy content. Phosphate is significant for various aspects of cellular metabolism of microalgae [24] and is essential for their growth. Prior studies have demonstrated that the HTL of algae biomass results predominantly in phosphate as well as nitrogen and other nutrients, such as K, Na, S, and Mg, in the HTL liquid phase [6,25–27]. The values of nutrients that are recovered in the HTL liquid phase depend heavily on the process parameter and initial algae composition (e.g., marine or freshwater species). Several studies that have been driven by the development of scalable algae-based biofuel production have already addressed nutrient recovery [28]. However, most research has focused on the feasibility of reusing the HTL liquid phase for algae cultivation to reduce the consumption of fertilizers for their growth [29]. Leng et al. [30] and Gu et al. [31] have provided a detailed overview of studies that concern the recycling of nutrients for algae cultivation. Generally, the HTL liquid phase has to be heavily diluted to avoid the inhibitory effect of organic compounds, such as phenols, furans, aromatic hydrocarbons, and nitrogenous compounds [26,32], on algal growth rate. Alba et al. [33] have indicated that the lack of essential nutrients (besides N and P) in the HTL liquid phase, which is enhanced by dilution, can lead to a reduction in the growth rate. Only a few studies have applied an integrated approach and precipitated the nutrients from the HTL liquid phase in the form of high-value

products, such as struvite. As noted above, McGinn et al. [12] have decoupled phosphate in the form of struvite from the HTL liquid phase to minimize the inhibition of algae growth through the presence of organic compounds. In addition, Shanmugam et al. [34] have used phosphate recovery via struvite precipitation as a pretreatment for anaerobic digestion of the HTL liquid phase and discovered that the biogas production from the struvite-recovered HTL liquid phase was 3.5x higher than that from the non-struvite-recovered HTL liquid phase.

Struvite precipitation is a well-known technology in wastewater treatment for the recovery of phosphate in the form of slow-release fertilizer [35]. This technique can be coupled with other processes. Some examples of coupling of struvite precipitation with HTL/HTC have been explained above, and another example can be found in reference [36]. The major benefit of struvite crystallization is the production of slow-release fertilizer that is established in the market, transportable, and suitable for long-term storage. Moreover, struvite production does not require severe process conditions; it is precipitated through pH adjustments to approximately pH 9, and the addition of a magnesium source, an ammonium source, or both, if necessary [37]. The production of struvite from HTL byproducts (HTL solid and HTL liquid phases) and its commercialization present an advantage in terms of the economic performance of fuel production and sustainability.

The aim of this study is to examine the feedstock-related application of HTL byproducts for nutrient extraction and evaluate the potential of phosphate recovery in the form of struvite in pilot-scale HTL bio-crude production. The specific research questions of this investigation are as follows: (1) To determine the relationship between feedstock and nutrient occurrence in HTL products at the pilot-scale; (2) to outline perspectives on the use of HTL byproduct streams to produce marketable fertilizer; and (3) to verify the possibility of efficiently recovering phosphate in the form of struvite from HTL byproducts by means of a laboratory-scale study.

2. Materials and Methods

2.1. Hydrothermal Liquefaction and its Products

The HTL products that were used in this study were produced at Aarhus University in Denmark by a continuous pilot-scale HTL reactor with a feed capacity of up to 100 L·h$^{-1,}$ and a total volume of the system of ~20 L. The detailed HTL reactor system description and the procedure can be found in reference [38]. In brief, it includes a feed introduction system, heat exchanger, trim heater, reactor, an oscillation system, a take-off system, and a product collection zone. Primary sewage sludge was collected in February 2018 from the primary treatment of wastewater at a plant in Viborg, while the *SPR* was purchased from Inner Mongolia Rejuve Biotech Co. Ltd. The initial dry matter content of feedstock slurries amounted to 4 wt% and 16.4 wt% for the PSS and *SPR*, respectively. Hydrothermal liquefaction was performed under sub-critical conditions at 220 bars and 350 °C. The flow rate of the slurries was 60 L·h^{-1}. The total duration of runs was 5 h and 6 h for the PSS and *SPR*, respectively. The HTL gaseous stream was separated from other HTL product streams in hydro-cyclone. The HTL oil phase that was produced was gravimetrically separated from the HTL liquid and HTL solid byproducts, which were subsequently separated by filtration [38]. The collected HTL oil, liquid, and solid phases were distributed to the HyFlexFuel partners for further investigation. The pre-dried feedstock and HTL solid phase that were obtained from Aarhus were dried at 105 °C and stored at room temperature for future handling. The HTL liquid phase that was obtained was immediately analyzed for elemental concentration and subsequently stored in a freezer at −24 °C prior to processing. The HTL oil phase that was obtained was stored at 4 °C. Figure 1 presents the simplified sample flow diagram and sample ID.

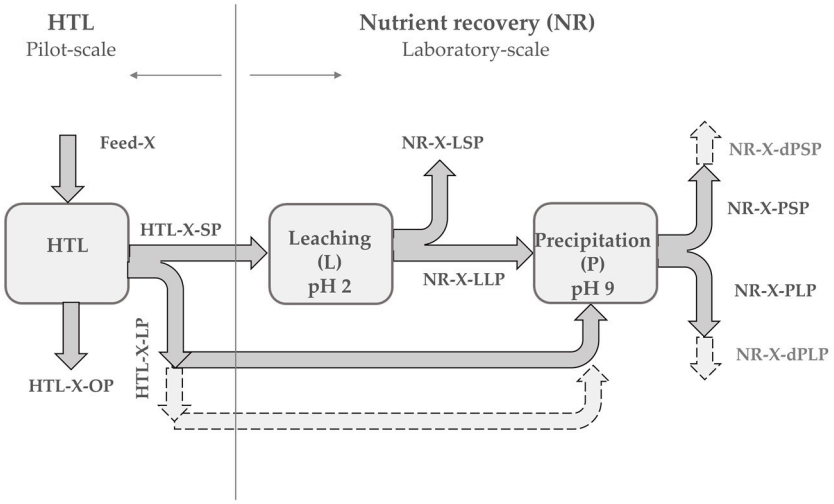

Figure 1. Simplified sample flow diagram and sample ID. SP solid phase; LP liquid phase; OP oil phase. X corresponds to primary sewage sludge (PSS) or *Spirulina* (*SPR*) and d to direct.

2.2. Phosphate Recovery.

2.2.1. Solubility Experiments

Solubility experiments were performed to evaluate the potential of phosphate release from the HTL solid phase if applied directly as a fertilizer or as a phosphate-containing source for subsequent extraction.

To identify the phosphate form that was presented in the HTL solid phase, the study applied semi-sequential fractionation extraction following the standards, measurements, and testing (SMT) harmonized protocol [39,40]. This procedure included 3 separate extraction proceedings to obtain 5 phosphorus fractions: Inorganic (IP) and organic (OP) phosphorus fraction; apatite inorganic (AP: Ca-bound) and nonapatite inorganic (NAIP: Associated to Al, Fe oxides, and hydroxides) phosphorus fraction; and, finally, total phosphorus (TP) as an overall characteristic. In addition, independent solubility behaviors of phosphate and other nutrients from the HTL solid phase in a range of acid-basic environments were studied. 10 mL of a leaching agent was added to 1 g of the dry HTL solid phase. The resulting slurry was shaken overnight at room temperature. After phase separation by centrifugation or filtration with 13 µm filter paper, the equilibrium pH of leachate was measured with a pH electrode HACH HQ40d. Two experimental setups were conducted. The 1st examined various leaching agents (1M HCl, 1M H_2SO_4, 1M NaOH, 1M citric acid). In the 2nd, sulfuric acid was used as a leaching agent, and their concentrations were varied (0.01M, 0.1M, 0.5M, 1M, 2M). The extraction capacity for phosphorus and other elements was calculated from the amount of the element that was extracted in leachate divided by the sample mass:

$$\text{Extraction capacity} = \frac{c_{\text{leachate}} \times V_{\text{leaching agent}}}{m_{\text{HTL-X-SP}}} \quad (1)$$

where c_{leachate} is the concentration of the element in leachate [mg·L^{-1}], and $V_{\text{leaching agent}}$ is the volume of the leaching agent [L].

To estimate the percentage of crop-available phosphate in the HTL solid phase, the study applied the calcium-acetate-lactate (CAL) extraction method (pH 4) [41] that was established in Germany for soil testing. Extraction was performed according to VDLUFA standard methods [42].

The elemental concentration in all extracts and leachates was measured by ICP-OES (Agilent 715). Analyses by SMT fractionation, all leaching tests, and the CAL extractions were conducted twice.

2.2.2. Struvite Production

To verify the possibility of phosphate recovery via struvite precipitation, the following procedure was conducted:

(1) 5 g of the dry HTL solid phase was suspended in 50 mL Milli-Q water to ensure pumpability at future large scales, and to reproduce the average output moisture condition from the HTL pilot plant. The slurry was subsequently leached with 1 molar sulfuric acid at pH 2 for 2 h (SI Analytics, TitroLine 7000)

(2) 5 mL of phosphate-rich leachate that was separated from the solid residual via filtration was mixed with the HTL liquid phase, which was high in ammonium ions, in a 1-to-6 ratio to guarantee an oversaturation state for struvite crystallization [37].

(3) After the addition of a previously estimated amount of $MgCl_2 \cdot 6H_2O$ to test the underdose and overdose scenarios of Mg^{2+}, the mixture was stirred for 2 h at constant pH 9 that was adjusted by 1M NaOH (SI Analytics, TitroLine 7000).

(4) Finally, the solid that precipitated was filtered with 0.13 µm filter paper and dried at 35 °C for future analysis. The HTL liquid phase from the *SPR* was also directly subjected to the struvite precipitation through supplementation of the magnesium source and maintained constant pH 9 for 2 h. Each trial was performed in duplicate.

The release rate and recovery rate for identifying the phosphate recovery performance were calculated as follows (sample ID presented in Figure 1):

$$\text{Release rate} = \frac{m_{HTL-X-SP} - m_{NR-X-LSP}}{m_{HTL-X-SP}} \times 100, \ [\%] \quad (2)$$

$$\text{Recovery rate} = \frac{(m_{\ NR-X-LLP} + m_{\ HTL-X-LP}) - m_{\ NR-X-PLP}}{(m_{\ NR-X-LLP} + m_{\ HTL-X-LP})} \times 100, \ [\%], \quad (3)$$

where m is the mass of phosphorus in the corresponding stream.

2.3. Analyses

2.3.1. Solid and Oil Phase

The inorganic elemental compositions of the feedstocks, the HTL solid and organic phases and the solid phases that were obtained during nutrient recovery were determined by ICP-OES (Agilent 715) after acid microwave-assisted digestion. The feedstock, HTL solid phase, and solid phase after leaching and precipitation (Figure 1) were digested by means of the INVERSE AQUA REGIA method in accordance with the procedure that has been described in reference [43]. The Feed-X, HTL-X-SP, and HTL-X-LSP were not completely dissolved during digestion since recalcitrant minerals, such as silica, were not affected; nevertheless, they are not of interest in the current study. Hence, in spite of the recognition of the applied procedure, the total element concentration may differ from that which was obtained due to the limitations of the digestion method. For digestion of the oil phase, the first step was to add 10 mL of 65% HNO_3 and 1 mL of 37% HCl to 100 mg of the organic phase. The solution was then digested in a microwave (CEM Discover) for 5 min at 220 °C. Subsequently, the completely dissolved samples were diluted to 25 mL with Milli-Q water. All digested solutions were correspondingly diluted with 1% HNO_3 to avoid matrix effects and to adjust to the calibration range of ICP-OES. The nitrogen content of the HTL oil and solid-phases was identified by an elemental analyzer (HekaTech, Euro EA). The ash content of the HTL solid samples was determined according to DIN 51719. The analyses were performed twice.

To specify the minerals that are associated with HTL solid phases and precipitates, the samples were characterized by powder x-ray diffraction (XRD). The diffraction patterns were recorded on a PANanalytical X'Pert Pro X-Ray diffractometer with a monochromatic CuKα radiation source. The raw

data were processed with Xpert-II software, and the mineral phases were identified with the Inorganic Crystal Structure Database (ICSD). The morphology of the precipitates was characterized by scanning electron microscopy (SEM; GeminiSEM 500 from Zeiss).

2.3.2. Liquid Phase

The HTL liquid phase, as well as liquid streams from the nutrient recovery (Figure 1), underwent analysis for pH, elemental concentration, and ammonium nitrogen (NH_4-N). NH_4-N was determined with the Hach-Lange cuvette test LCK 304. The inorganic element content was measured with ICP-OES (Agilent 715) by injection diluted 1-to-10 with 1% HNO_3 HTL liquid samples. The nitrogen content was determined by an elemental analyzer (HekaTech, Euro EA), and the pH was measured by HACH HQ40d. The analyses were conducted twice.

3. Results and Discussion

3.1. Nutrient Distribution in Feedstocks and Between HTL Products

Table 1 illustrates the difference between PSS and *SPR* in terms of composition. The ash content, which reflected the inorganic matter of *SPR* (5.8 wt%), was similar to those reported by other studies [22,38,44,45] and significantly lower than the ash content of PSS (19.3 wt%). Its value in the literature ranged from 7.5 wt% [14,15] to over 30 wt% [46,47]. This variation was linked to the strong dependencies of the composition of PSS on the sewage sludge source and treatment techniques of wastewater. The nutrient content in the *SPR* mainly reflected the elemental concentration of the cultivation medium that was used [48]. Thus, the analytes of potassium (1.7 wt%), phosphorus (1.1 wt%), sodium (0.4 wt%), and magnesium (0.3 wt%) constituted the main inorganics of *SPR*, which (with the exception of magnesium) was in accordance with previous studies [26]. By contrast, calcium (4.0 wt%), phosphorus (2.1 wt%), iron (0.6 wt%), and aluminum (0.4 wt%) constituted the major inorganic composition of PSS [49]. The higher protein content in *SPR* [50] resulted in higher nitrogen and sulfur contents compared to those in PSS.

Table 1. Nutrient distribution in feedstocks and between hydrothermal liquefaction (HTL) products (mean value (MV) ± standard deviation (SD) of two replicates).

Sample ID	Ash	P	N	K	S	Na	Mg	Ca	Fe	Al
-	wt%	mg·g^{-1}	wt%	mg·g^{-1}	mg·g^{-1}	mg·g^{-1}	mg·g^{-1}	mg·g^{-1}	mg·g^{-1}	mg·g^{-1}
Feed-PSS [a]	19.3	21.2	2.9	2.2	3.7	2.7	1.4	40.2	6.4	3.6
±	0.6	2.5	0.0	0.4	0.1	0.6	0.2	4.7	0.4	0.2
Feed-*SPR* [a]	5.8	11.1	11.1	17.1	8.0	4.5	3.2	1.1	0.7	0.1
±	0.0	1.1	0.0	1.7	0.7	0.5	0.3	0.1	0.1	0.0
HTL-PSS-OP [b]	28.4 [c]	28.5	2.0	0.7	2.9	0.3	3.1	48.2	7.6	4.2
±		3.9	0.1	0.1	0.4	0.0	0.4	11.8	0.6	0.7
HTL-*SPR*-OP [b]	6.6 [c]	<0.1	6.5	<0.1	8.3	<0.1	<0.1	<0.1	0.9	<0.1
±			0.1		0.7				0.0	
HTL-PSS-SP [a]	79.6	99.2	0.9	2.6	2.0	1.0	14.5	220.4	14.7	18.4
±	0.2	1.8	0.0	0.1	0.1	0.0	0.1	15.4	3.4	0.0
HTL-*SPR*-SP [a]	32.0	58.2	5.3	15.9	7.8	11.4	38.4	22.6	7.2	1.8
±	0.2	0.8	0.0	0.3	0.4	0.2	0.8	0.6	0.1	0.0
	wt%	mg·L^{-1}	wt%	mg·L^{-1}	mg·L^{-1}	mg·L^{-1}	mg·L^{-1}	mg·L^{-1}	mg·L^{-1}	mg·L^{-1}
HTL-PSS-LP	NA [d]	15.8	0.1	97.6	54.3	157.8	13.9	3.2	<0.3	<1.5
±		1.4	0.0	5.4	0.4	8.5	1.4	0.1		
HTL-*SPR*-LP	NA [d]	1082.4	1.1	2243.7	403.4	541.0	0.2	4.5	0.9	<1.5
±		58.0	0.2	176.6	22.5	53.7	0.1	0.5	0.1	

[a] on dry basis; [b] analyzed as received; [c] from [38]; [d] not analyzed.

Differences in the composition and structure of feedstocks resulted in disparate distributions of nutrients in the HTL products (Table 1). The inorganics that were found in the oil phase can have an impact on upgrading to fuel [51–53]. For example, phosphor- and iron-containing species could settle on the upgrading catalyst, thereby blocking access to the catalyst interior and thus deactivating it. The pollution of the HTL oil phase with nitrogen also appears to inhibit the upgrading step [54]. The low level of sulfur in the HTL oil phase could have a negative effect on the activity of conventional sulfided upgrading catalysts, e.g., CoMo catalyst [52,55]. In the *SPR* oil phase, iron was present in abundant concentrations (0.1 wt%). These results concur with previous studies of HTL of microalgae [44,56,57]. Iron-associated proteins that were present in microalgae biomass [58] appeared to be stable to decomposition during HTL and can be recovered in bio-crude as iron-porphyrins [51]. The demineralization regarding iron was difficult [59] and required more detailed investigation. The PSS oil phase was contaminated primarily by the elements of calcium (4.5 wt%) and phosphorus (2.8 wt%). The presence of inorganic elements in HTL-PSS-OP may be related to solid particles [60]. To investigate this hypothesis, the PSS oil phase was dissolved in ethanol, and the measurement of the particle size distribution was conducted with dynamic image analysis after destroying agglomerates in an ultrasonic bath. It was detected that a noticeable number of particles with a mean diameter of 38 µm were suspended in the PSS oil phase (see Figure S1). In contrast, by the same method, a number of solid particles in HTL-*SPR*-OP were negligible. The transport of solid particles in the oil phase is not yet known. Their content could be reduced by, for example, an in-line filtration system during HTL, which was not in operation during the present study [38,61].

A proportion of biomass phosphorus (as phosphate) was recovered in both the HTL solid and liquid phases. The HTL solid phase was the main reserve of phosphate from the PSS, as in Marrone's study [15], while the phosphate from the *SPR* was found in both the HTL solid and liquid phases (Table 1). Moreover, the content of phosphorus in HTL-*SPR*-LP was in the range of previous studies [26,32]. The distribution of phosphate can relate to the presence of other dissolved multivalent metal ions, such as $Ca^{2+,}$ Mg^{2+}, Al^{3+}, and $Fe^{2+/3+}$ [6,62], in the reaction solution that tended to precipitate in the form of phosphate salts under a subcritical condition [63–65]. Their high concentration can shift the phosphate from the liquid phase to the solid phase. Therefore, the considerable concentration of metal ions (primarily Ca^{2+}) in PSS compared to *SPR* could be responsible for the recovery of phosphate in the HTL solid phase. While the multivalent ions demonstrated a tendency to precipitate under the studied hydrothermal conditions—which was reflected in the fact that calcium, magnesium, iron, and aluminum were mainly recovered in the HTL solid phase—the monovalent ions (K^+, Na^+) remained dissolved in the HTL liquid phase. A similar tendency has been described in references [66,67]. The nitrogen that was recovered in the HTL liquid phase, which resulted from the degradation of proteins under hydrothermal conditions [15,26], was clearly higher for HTL-*SPR*-LP than for HTL-PSS-LP. The different levels of nitrogen (as ammonium) in the HTL liquid phase between PSS and *SPR* resulted in different pH levels [68]. The pH of the HTL liquid phase from the processing of *SPR* became basic (pH 8.5), and that of PSS became neutral (pH 7.0), which in turn induced alteration of the mineral solubility.

Figure 2 presents the estimated elemental balance for the experimental HTL pilot plant runs of PSS and *SPR*. By taking into account the mean yield of the oil phase (24.5 wt% and 32.9 wt% on a dry basis [38]), the dry matter content of feedstock slurries, the flow rate of slurries, and the total duration of runs, the elemental balance was calculated from the average elemental content in the HTL products that were obtained after the reactor runs (Table 1). The density of slurries was calculated with consideration to the percentage of solids in the slurry and by a solid density of 500 $kg \cdot m^{-3}$ [38]. It is important to note that the yields of gas, liquid, and solid HTL byproducts were not directly measured at this stage of the development of the HTL pilot plant. The yields for the gas and solid phases, which were determined on the basis of the dry matter of feedstock, were taken from previous studies at the batch system as average values. The yields for the HTL solid and gas phases were assumed to be 10 wt% and 14 wt% [47,69] for PSS and 5 wt% and 20 wt% [9,44,47,50] for *SPR*. The amount of the HTL liquid phase after the run was calculated as the difference between the mass of feedstock slurry and

the mass of oil, solid, and gas phases that were produced in each run. The percentage of the respective elements for the HTL runs of PSS and *SPR* was calculated from the division of the mean amount of the element in the corresponding phase by the mean amount of this element in the biomass feedstock. The SD of the percentage was calculated from the SD of the elemental content in the biomass feedstock and the HTL product (Table 1); the SD of the yield of the HTL product was not taken into account due to lack of information.

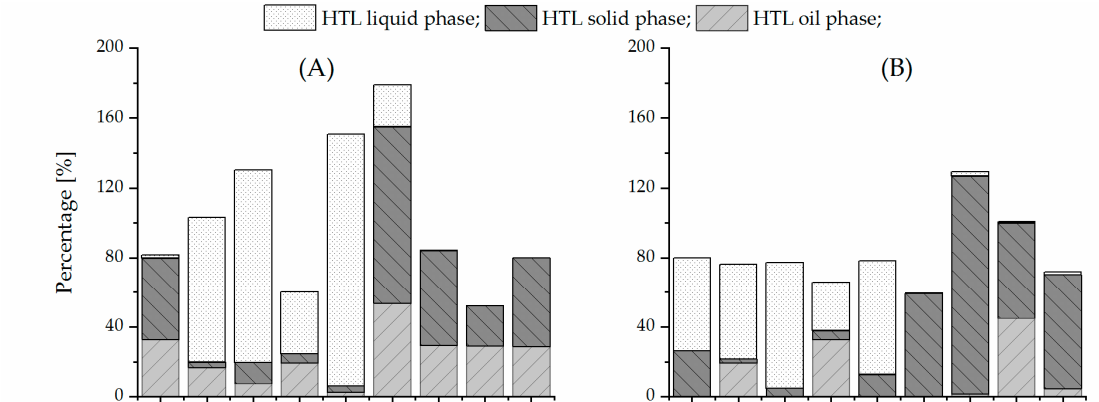

	P	N	K	S	Na	Mg	Ca	Fe	Al
HTL liquid phase	1.8	83.1	110.8	35.6	144.5	23.9	0.2	0.0	0.0
±	0.3	0.4	21.4	1.3	33.3	4.1	0.0	0.0	0.0
HTL solid phase	46.8	3.0	12.1	5.4	3.7	101.4	54.8	23.0	51.3
±	5.6	0.0	2.3	0.3	0.8	14.2	7.5	5.5	2.9
HTL oil phase	32.9	16.8	7.4	19.3	2.5	53.6	29.3	29.2	28.7
±	6.0	0.8	1.8	3.0	0.6	10.2	8.0	2.9	5.0

P	N	K	S	Na	Mg	Ca	Fe	Al
53.6	54.7	72.6	27.8	65.7	0.0	2.4	0.7	1.5
6.0	9.9	9.2	2.9	9.7	0.0	0.3	0.1	0.5
26.1	2.4	4.7	5.0	12.5	59.2	125.2	54.9	65.0
2.6	0.0	0.5	0.5	1.4	5.6	12.1	8.5	0.0
0.1	19.3	0.1	32.9	0.2	0.2	1.6	45.0	4.8
0.0	0.3	0.0	4.1	0.0	0.0	0.5	7.2	0.5

Figure 2. Estimated elemental balance for HTL runs of PSS (**A**) and *SPR* (**B**) (MV ± SD; error bars are not shown in the figure).

Such assumptions might lead to an over- or underestimation of the elemental mass balance. In general, a lower balance closure was observed for the HTL run of PSS than for the HTL run of *SPR*. The mass balance for HTL of PSS (Figure 2) indicated an overestimation of good soluble elements, such as potassium and sodium, and underestimation of poor soluble elements, such as phosphorus, calcium, iron, and aluminum. The causes for this over- or underestimation are unclear but might originate from an overestimation of the amount of the HTL liquid phase or an overestimation of the elemental content by, for instance, evaporation of some HTL liquid phase during sampling (for K and Na) or from fouling and deposition in the reactor (for P, Ca, Fe, and Al). The especially high overestimation of magnesium in PSS is questionable and might be due to contamination of the pilot plant from previous runs. The calculated mass balance for the HTL run of *SPR* (Figure 2) is more or less closed. Only the balance for calcium exceeded 100%, which may be linked to the dissolution of Ca deposits in the reactor. In addition, the sampling of a multi-phase system is always challenging since the ratio of the phases might not be correct in each sample. Despite the over- and underestimation, several general tendencies regarding mass balance can be identified. The preliminary mass balance can assist in selecting a promising strategy for nutrient extraction.

The phosphorus balance was closed at 82% and 80% for the HTL run of PSS and *SPR*. The balance suggests that approximately half of the phosphorus from the processed *SPR* was extracted in the HTL liquid phase, while half of the phosphorus from PSS in the HTL solid phase. The smaller fraction of phosphorus from *SPR* was recovered in the HTL solid phase, and from PSS in the bio-crude. The phosphorus distribution determines the possibility of using the HTL solid and liquid phases as an indirect or direct source of phosphates in the case of HTL of PSS and *SPR*, respectively. Nonetheless, there appears to be a strong tendency to recover phosphates with the PSS bio-crude. As mentioned, a substantial load of particles with a mean diameter of 38 µm were impurifying the crude oil. Therefore, the phosphate remains in mineral form and can be filtered from the crude oil. The data for nitrogen also provided an acceptable balance. Approximately four-fifths of the recovered nitrogen was in the HTL

liquid phase for the HTL run of PSS, and three-fourths for the HTL run of *SPR*. Thus, the availability of nitrogen for recovery from the liquid phase was increased by HTL. Magnesium, calcium, iron, and aluminum from PSS exhibited the same tendency as the phosphorus distribution. Meanwhile, these metals from *SPR*, with the exception of iron, were recovered primarily in the HTL solid phase. The occurrence of iron in the form of recalcitrant porphyrin in bio-crude has already been discussed. The majority of the potassium and sodium that were initially present in PSS and *SPR* was found in the HTL liquid phase, which was consistent with previous studies on batch systems [66].

3.2. Strategy of Phosphate Recovery

The mass balance that has been presented in Section 3.1 demonstrates that the HTL solid byproduct could be an appropriate point for phosphate recycling and reuse. In view of the aforementioned disadvantages, this work does not further consider the direct use of the HTL liquid. The HTL solid phase from PSS and *SPR* with the agronomic relevant composition (N-P_2O_5-K_2O) of 0.9-22.7-0.4 and 5.3-13.3-1.9 (Table 1), respectively, may represent a material with properties that are relevant to the application as a fertilizer. For this purpose, the phosphate must be released from the HTL solid phase to become available for the crops. The release behavior of phosphate is related to its form.

Figure 3 presents the respective content of the various forms of phosphate in the HTL solid phases from PSS and *SPR*, as well as the percentage of crop-available phosphate. The phosphate was mainly present in IP form; in both cases, the OP amounted to less than 1%. Moreover, IP consisted mainly of AP (97 wt% and 65 wt% for HTL-PSS-SP and HTL-*SPR*-SP, respectively). The phosphate form distribution was in line with those in previous studies of phosphate behavior under hydrothermal conditions [70–73]. The higher percentage of AP in the HTL solid phase from PSS could relate to the higher level of calcium in PSS (Table 1) compared to in *SPR* [73]. The Ca-bound phosphate was the most prevalent phosphate form in HTL-PSS-SP, which was consistent with XRD analysis. Such analysis concluded that calcium phosphate with inclusions of sodium and magnesium ($(Ca_{3.892}Na_{0.087}Mg_{0.021})(Ca_{5.491}Na_{0.121}Mg_{0.028})(PO_4)_{5.1}$) was the most abundant phosphate crystalline mineral in the HTL solid residual from PSS (see Figure S2). This finding was consistent with findings of minerals by other researchers after hydrothermal treatment of biomass that is rich in metals [43,74,75]. In turn, the recorded diffraction patterns of HTL-*SPR*-SP corresponded to a dittmarite mineral ($NH_4MgPO_4 \cdot H_2O$) (see Figure S2). In contrast, Roberts et al. [64] have detected hydroxyapatite after HTL of microalgae biomass. The differences may be explained by the lower calcium content in *SPR* and the presence of calcium phosphate in HTL-*SPR*-SP in an amorphous form [74] that cannot be detected by XRD. The CAL-P extraction illustrated that these minerals might not be used directly as fertilizer. The crop-available form of phosphate was only 1 wt% in HTL-PSS-SP and 31 wt% in HTL-*SPR*-SP. Furthermore, previous studies [17,18] have identified enrichment of the HTL solid phase with heavy metals. Thus, a concentration of phosphate in high-value fertilizer, such as struvite was required. Struvite production through the approach of precipitating phosphate that was released from the HTL solid phase [19] does not seem difficult to implement at the industrial scale and is investigated further in the next section.

3.3. Phosphate Recovery

3.3.1. Release of Phosphate from the HTL Solid Phase

Section 3.2 has identified the HTL solid phase as a phosphate-containing source. The release of phosphate from mineral phases by wet chemical extraction (also known as leaching) is the most common technique, as it offers high efficiency and low energy demand. On the other hand, the consumption of the leaching agent and the co-dissolution of inorganic species other than phosphate salts can negatively affect the extraction. The leaching study was carried out with the aim of identifying optimal conditions for the production of phosphate-rich leachate with high purity for struvite precipitation.

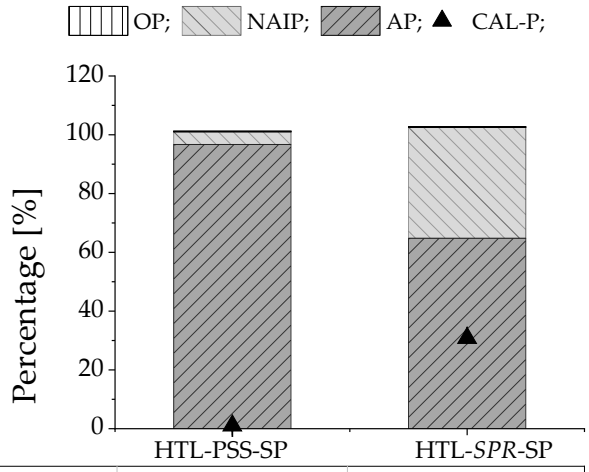

	HTL-PSS-SP	HTL-*SPR*-SP
OP	0.2	0.1
±	0.0	0.0
NAIP	4.4	37.8
±	0.4	2.3
AP	96.7	64.8
±	5.5	2.5
CAL-P	1.0	30.8
±	0.0	0.6

Figure 3. Different forms of phosphate as well as the crop-available form of phosphate in HTL solid phase (MV ± SD of two replicates; error bars are not shown in the figure). The percentage was calculated as follows: (AP(IP, OP, or CAL-P)/TP) × 100%.

Figure 4a indicates that sulfuric and hydrochloric acids provided a considerable phosphate extraction capacity for the HTL solid phase from both PSS and *SPR* (equilibrium pH of leachate <2). The application of NaOH as a leaching agent was limited. The environmentally beneficial citric acid demonstrated a lower efficiency than that of mineral acids for phosphate recovery from HTL-PSS-SP. The reason for this lower efficiency could be the precipitation of secondary nonapatite phosphate in the case of citric acid. Together with calcium phosphates, other acid-soluble compounds that present in HTL-PSS-SP, such as $CaCO_3$ and Mg-, Fe-, and Al-containing compounds, might be decomposed as well. The released from calcium phosphate PO_4^{3-} ion can instantly bind with available aluminum or iron ions that have a high affinity for phosphate and precipitates, such as secondary Al- and Fe-phosphate salts. According to a study of phosphate solubility by Stumm and Morgan [76], when decreasing the pH, the Ca-phosphate dissolved first, with the Al-phosphate and Fe-phosphate following, respectively. Almost complete acidic phosphate dissolution can be expected at pH < 2 [77,78]. Thus, the precipitation of secondary Al- and Fe-phosphate salts may explain why weaker citric acid (equilibrium pH of leachate >2) exhibited a poorer extraction performance compared to sulfuric and hydrochloric acid for HTL-PSS-SP. This suggestion was also supported by the higher extraction capacities of aluminum and iron ions with H_2SO_4 than with citric acid. For sulfuric acid as a leaching agent, the extraction capacities of aluminum and iron were 5 $mg \cdot g^{-1}$ and 20 $mg \cdot g^{-1}$, respectively. For citric acid, the capacities were 2 $mg \cdot g^{-1}$ and 10 $mg \cdot g^{-1}$, respectively. In contrast, the extraction efficiency of citric acid for HTL-*SPR*-SP was comparable to those of sulfuric and hydrochloric acids. This finding can be linked to the higher solubility of the phosphate forms in HTL-*SPR*-SP compared to the phosphate forms in HTL-PSS-SP (Figure 3). Furthermore, the contents of aluminum and iron in the HTL solid phase from *SPR* were lower (0.2 wt% and 0.7 wt%, respectively) than from PSS (1.8 wt% and 1.5 wt%, respectively). The molar relation between metal ions and phosphate in the HTL solid phase from *SPR* (Al/P ~0.03 and Fe/P ~0.07) was lower than that from PSS (Al/P ~0.21 and Fe/P ~0.08), which can result in less co-precipitation of secondary Al- and Fe-phosphate salts [77]. While citric acid provided a high extraction capacity for HTL-*SPR*-SP, its application may be limited by its negative effect on subsequent precipitation [79]. Figure 4a conveys that sulfuric acid is more selective to phosphate

release compared to other leaching agents. Significantly less calcium was found in the extract with the application of sulfuric acid, which could relate to the simultaneous co-precipitation of calcium sulfate (gypsum) [80]. This co-precipitation can be seen specifically in the decreasing calcium ion concentrations with increasing concentrations of sulfuric acid in Figure 4b. Large-scale use of sulfuric acid is beneficial from an economic perspective because it offers a low cost as a byproduct of the desulfurization of natural gas and petroleum. Consequently, sulfuric acid was selected as the leaching agent for the following study.

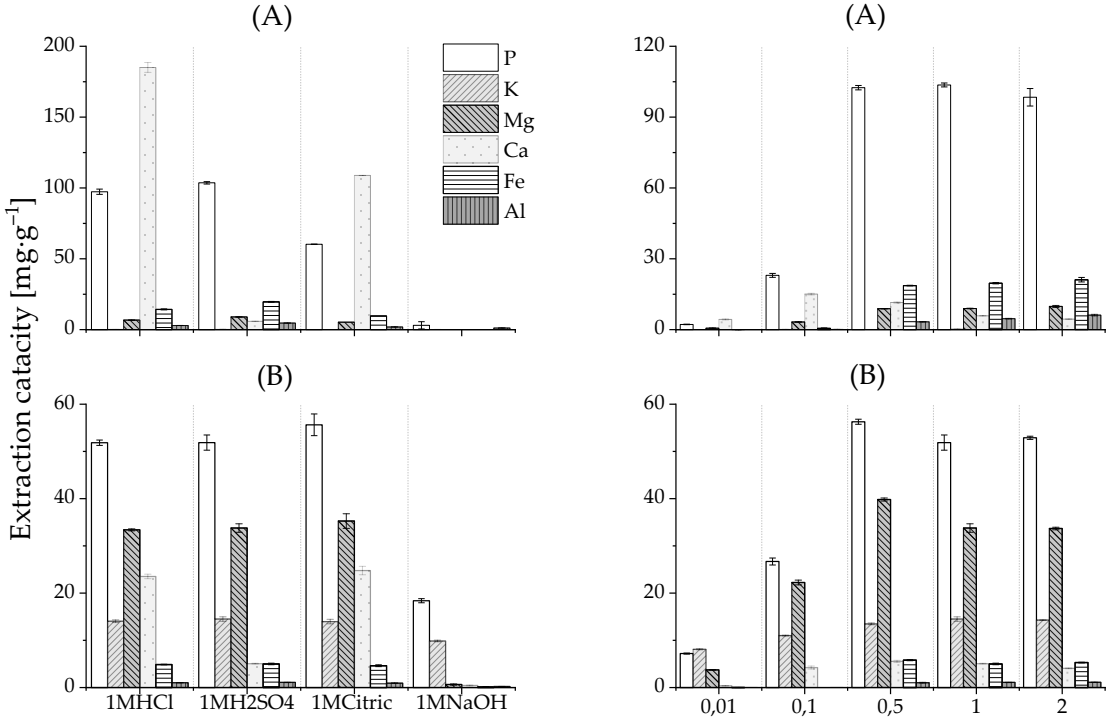

(**a**) Leaching Agent (**b**) H_2SO_4 concentration

Figure 4. Effect of the leaching agent (**a**) and H_2SO_4 concentration (**b**) on the extraction capacity of elements P, K, Mg, Ca, Fe, and Al for the HTL solid phase from PSS (A) and *SPR* (B).

Phosphate was extracted at multiple sulfuric acid concentrations. Figure 4b indicates that an acid concentration of 0.1M provided incomplete extraction (22% in the case of HTL-PSS-SP and 47% in the case of HTL-*SPR*-SP). The maximum extraction capacity from the HTL solid phase was achieved at 0.5M. Higher acid concentrations, which imply an increase of H^+ per g of the HTL solid phase, did not result in a significant improvement in extraction results. The estimation of acid consumption for the phosphate release was essential for the technical feasibility of phosphate recovery technologies. The amount of acid that is required depends on the chemical composition of the HTL solid phase. Calcium phosphate is its main constituent (Figure 3) and reacts essentially with acid; thus, it is the main acid consumer. The literature has reported an average acid consumption for solid residuals that are rich in calcium phosphate was around 3 mol H^+ pro mol P [77,80,81]. If one assumes an average consumption of sulfuric acid of 3 mol H^+ pro mol P to dissolve the phosphates in the HTL solid phase at a given liquid-to-solid ratio (10:1), then sulfuric acid with concentrations of 0.5M and 0.3M should be sufficient to release phosphate from HTL-PSS-SP and HTL-*SPR*-SP, respectively. These calculated concentrations are positively reflected in the experimental data in Figure 4b.

In the context of sustainability, the potential to recycle the remaining acid-insoluble solid residue should also be considered. This acid-treated residual contains low concentrations of phosphorus. The concentrations of other major elements are also altered. The byproduct of leaching of the HTL solid phase from PSS could be used, for example, for the production of activated carbon [21] or as pozzolan

in concrete [82]. Of course, the high sulfur content due to gypsum precipitation in the leaching step (with sulfuric acid) warrants attention. Further work with acid-washed HTL residues is required to improve the current understanding of this material.

3.3.2. Phosphate Precipitation in the Form of Struvite

This section examines phosphate separation in the form of struvite ($MgNH_4PO_4 \cdot 6H_2O$) by mixing phosphate-rich leachate with the HTL liquid phase that contains an ammonium ion. Ammonium nitrogen (NH_4-N) amounted to 320 mg·L^{-1} in HTL-PSS-LP and to 6800 mg·L^{-1} in HTL-*SPR*-LP. The measured concentration can be lower than the real one because of the possible loss of some ammonium during the thawing of the liquid samples. Since half of the phosphate from *SPR* (Figure 2) remains after HTL in the liquid phase, the possibility of direct struvite crystallization from the HTL liquid phase was examined. Table 2 presents the nutrient distribution in process streams that circulated in nutrient recovery (Figure 1), while Table 3 illustrates the performance of the nutrient recovery.

Table 2. Nutrient distribution in the streams circulated by phosphate precipitation.

Sample ID	P	N	K	Mg	Ca	NH_4-N
-	mg·g^{-1}	wt%	mg·g^{-1}	mg·g^{-1}	mg·g^{-1}	mg·g^{-1}
NR-PSS-LSP	47.5	NA [a]	2.1	7.9	109.8	-
±	3.0		0.1	0.2	5.8	
NR-*SPR*-LSP	7.2	NA [a]	2.5	2.7	25.5	-
±	0.6		0.1	0.4	0.1	
NR-PSS-PSP	97.9	3.9	1.2	75.2	15.7	-
±	8.2	0.0	0.2	6.0	2.2	
NR-*SPR*-PSP	90.0	5.3	2.2	68.8	7.7	-
±	8.6	0.0	0.2	6.8	0.5	
NR-*SPR*-dPSP	95.6	5.2	1.4	87.1	0.2	-
±	4.9	0.0	0.2	11.5	0.0	
-	mg·L^{-1}	wt%	mg·L^{-1}	mg·L^{-1}	mg·L^{-1}	mg·L^{-1}
NR-PSS-LLP	3890.1	NA [a]	5.0	466.3	1066.3	NA [a]
±	146.9		0.0	21.7	7.5	
NR-*SPR*-LLP	4309.1	NA [a]	1087.0	2232.2	440.6	NA [a]
±	33.4		25.8	2.5	5.1	
NR-PSS-PLP	5.2	NA [a]	51.4	846.0	119.9	53.5
±	0.2		1.3	30.3	10.8	7.5
NR-*SPR*-PLP	449.4	NA [a]	1100.6	0.1	9.4	4080.0
±	44.2		119.7	0.0	0.6	510
NR-*SPR*-dPLP	1.0	NA [a]	1063	292.2	3.8	44,650
±	0.0		75.7	57.1	1.3	525

[a] not analyzed.

The release rate of phosphate from the HTL solid phase from PSS was lower than that from HTL solid phase from *SPR*. The previous section has suggested that approximately 3 mol H^+ pro mol P was required to dissolve the phosphate from the HTL solid phase from PSS. To set and maintain pH 2, 2.7 mL H_2SO_4 pro g of the HTL solid phase from PSS was piped into the system. Assuming complete dissociation of H_2SO_4 corresponded to approximately 1.6 mol H^+ pro mol P at the given liquid-to-solid ratio. There does not seem to be sufficient H^+ to provide complete dissolution of primary and secondary phosphate. In the case of *SPR*, the H_2SO_4 guided into the system was equivalent to approximately 2 mol H^+ pro mol P. It was sufficient to result in the dissolution of a major part of the phosphate and conforms to the previously specified considerations.

Table 3. Performances of phosphate recovery.

X	Unit	PSS	*SPR*	d*SP*
Leaching				
HTL-X-SP/H_2O	-	1:10	1:10	-
1M H_2SO_4/HTL-X-SP	$mL \cdot g^{-1}$	2.7 ± 0.3	2.2 ± 0.1	-
Extraction capacity of P	$mg_P \cdot g^{-1}{}_{sp}$	49.4 ± 2.3	52.2 ± 0.1	-
Release rate P	%	49.9 ± 2.2	90.2 ± 0.8	-
Precipitation				
Leachate/HTL-X-LP	-	1:6	1:6	-
NH_4^+:PO_4^{3-}	$mol \cdot mol^{-1}$	1.1	8.4	13.9
Mg^{2+}:PO_4^{3-}	$mol \cdot mol^{-1}$	2.6	0.4	1.5
Mg^{2+}:Ca^{2+}	$mol \cdot mol^{-1}$	12.3	11.8	467
Recovery rate P	%	99.0 ± 0.0	66.5 ± 2.9	99.9 ± 0.0
Recovery rate Mg	%	22.6 ± 3.0	99.9 ± 3.0	67.9 ± 4.3
NH_4-N recovery	%	79.4 ± 2.8	19.4 ± 9.3	8.0 ± 4.4
Masse precipitate/P in initial mix solution	$g \cdot g^{-1}{}_P$	11.1 ± 0.2	5.8 ± 0.1	9.3 ± 0.0

The recovery rate of phosphorus from the mix solution was approximately 99% and 66% for PSS and *SPR*, respectively, and approximately 99.9% for direct precipitation from the HTL liquid phase of *SPR*. The pH, molar ratio of the participating ions (PO_4^{3-}, Mg^{2+}, NH_4^+), and presence of foreign ions (e.g., Ca^{2+}) are among the major parameters that affect the struvite crystallization [83]. The formation of struvite occurs with the creation of supersaturation (index of the deviation of a dissolved salt from its equilibrium), which is the driving force of crystallization. Supersaturation may be achieved by increasing any or all concentrations of ammonium, magnesium, phosphate, and pH in the solution. In general, pH 9 is optimal for struvite precipitation [84]. To attain oversaturation in the mixed solution (spontaneous formation of struvite), the phosphate-rich leachate was mixed with the HTL liquid phase that was high in ammonium ions in a 1-to-6 volume ratio. The results were the molar ratios of 1.1 and 8.4 for PSS and *SPR*, respectively. The molar ratio of NH_4^+:PO_4^{3-} in the HTL process water of *SPR* was 13.9. The excess of ammonium is beneficial for struvite crystallization [85,86] and could positively affect the purity of the precipitate, as supported by the fact that the nitrogen content in the precipitate from *SPR* (5.3% and 5.2%) was higher than from PSS (3.9%) and within range of the theoretical value of 5.7%. In contrast, the overdose of ammonium resulted in a low recovery rate of ammonium ions (only 19% and 8% for *SPR* compared to 79% for PSS). The magnesium-to-phosphate molar ratio was also key during struvite crystallization. The magnesium content in leachate and process water was low relative to the phosphate content. Thus, the Mg^{2+}:PO_4^{3-} ratio had to be adjusted by the addition of a magnesium source, which provided the Mg^{2+} that was required for oversaturation and offsets the negative effect of the calcium ion, which competed with the magnesium ion for the phosphate ion [83]. In the case of PSS, the Mg^{2+}:PO_4^{3-} ratio was adjusted to approximately 2. The underdose and overdose scenarios were compared for *SPR* as feedstock with a low concentration of Ca^{2+}. In the case of an underdose of magnesium, the recovery rate was approximately 66%, which indicated that the magnesium ion was a limiting factor for struvite precipitation. This finding was in line with reference [86]. Thus, to improve the performance of phosphate recovery for *SPR*, a higher magnesium ion dose was necessary. However, it is notable that the optimal design of phosphate recovery entails a compromise between the performances and chemical consumption.

The percentage of each element (Table 2) in the precipitate was compared with the theoretical value for pure struvite as a reference (12.6 wt% P; 5.7 wt% N; 9.9 wt% Mg). It can be concluded that the precipitate correlated well with struvite. This suggestion was further confirmed by the XRD analysis. The XRD patterns of the precipitate matched the reference struvite (see Figure S3). Figure 5 presents the SEM image of the precipitate that was obtained. The SEM images revealed coarse, irregularly shaped crystals of various sizes. The most commonly observed crystals in the precipitate from PSS

had an average length of 10 µm. The crystals were larger in the case of *SPR*. An excess of ammonium ions may account for the larger size, as already illustrated by other research [83,87]. In addition to the struvite crystals, other solid precipitates were found (marked with yellow arrow). This co-precipitates might be amorphous calcium phosphate. The smaller amount of Ca^{2+} in the case of *SPR* can result in fewer impurities in the form of calcium phosphate, as evident in the SEM images.

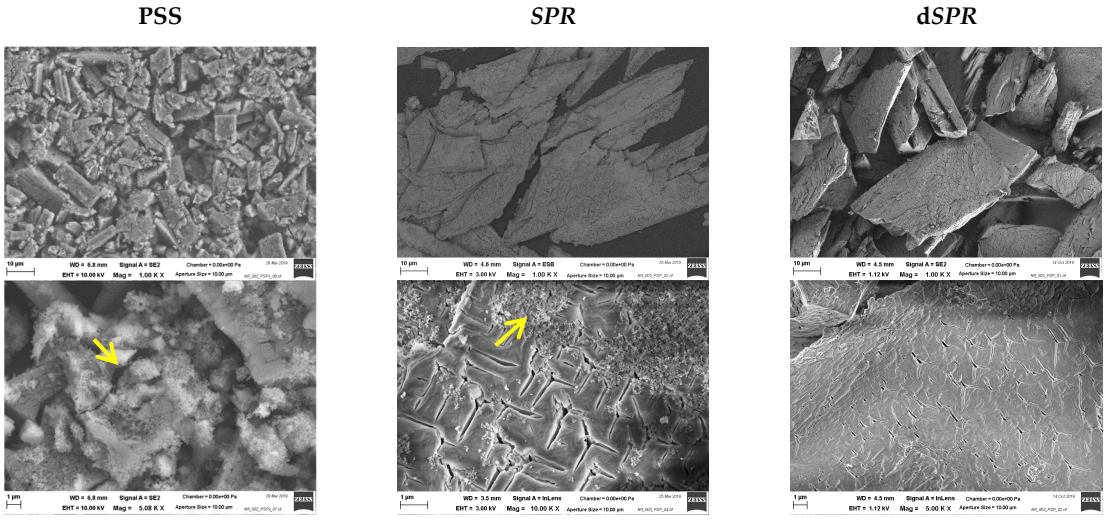

Figure 5. Scanning electron microscopy images of the precipitates that were obtained by mixing phosphate-rich leachate from the HTL solid phase with the HTL liquid phase (PSS and *SPR*) and by direct precipitation from the HTL liquid phase (d*SPR*). Solid precipitates different from struvite are marked with a yellow arrow.

It has been indicated that acid dissolving of phosphate followed by precipitation of struvite is an effective approach for HTL-based phosphorus recovery. To scale up and optimize the performance of this approach in terms of the quantity of struvite that it generates, the characteristics (size and purity) of the precipitate, and the consumption of chemicals, it is necessary to gain additional insight into struvite formation, which requires a detailed study.

3.3.3. Overall Consideration of Process and Mass Flow of Macronutrients

The phosphate recovery performance in the laboratory-scale study and the elemental balance that was calculated for the HTL pilot plant were used to calculate the mass flow diagram of macronutrients during the HTL coupling with nutrient recovery (see Figure 1). The calculated mass balance can help to reduce the process development time and identify future research potential.

The mass flow for PSS (Figure 6a) implies a relatively low recovery rate of phosphate from unprocessed PSS in the form of struvite. It can firstly be linked to the recovery of a considerable amount of phosphate in the HTL oil phase and, secondly, to the non-optimal efficiency of the leaching step. The increase of acid consumption (Section 3.3.2) to approximately 3 mol H^+ pro mol P might lead to the complete dissolution of the phosphate and an improvement in leaching efficiency. Moreover, the release of more phosphate may result in an increase in the HTL liquid phase and the Mg source consumption to cover the corresponding ion ratio as well as in the NaOH consumption for adjusting the pH. For example, an increase of 1M H_2SO_4 up to 1 $L{\cdot}h^{-1}$ (corresponds to 3 mol H^+ pro mol P) can require an increased HTL liquid phase to provide NH_4^+:PO_4^{3-} of 1.6 up to 55 $L{\cdot}h^{-1}$. This amount may conflict with the amount of the liquid phase that originates from HTL (calculated at approximately 57 $L{\cdot}h^{-1}$). The increase in chemical consumption that [88] has been identified as a major part of struvite production costs could result in heightened operating costs. The improvement of nutrient performance necessitates a trade-off between the amount and quality of struvite and the consumption of ammonium and magnesium sources as well as NaOH.

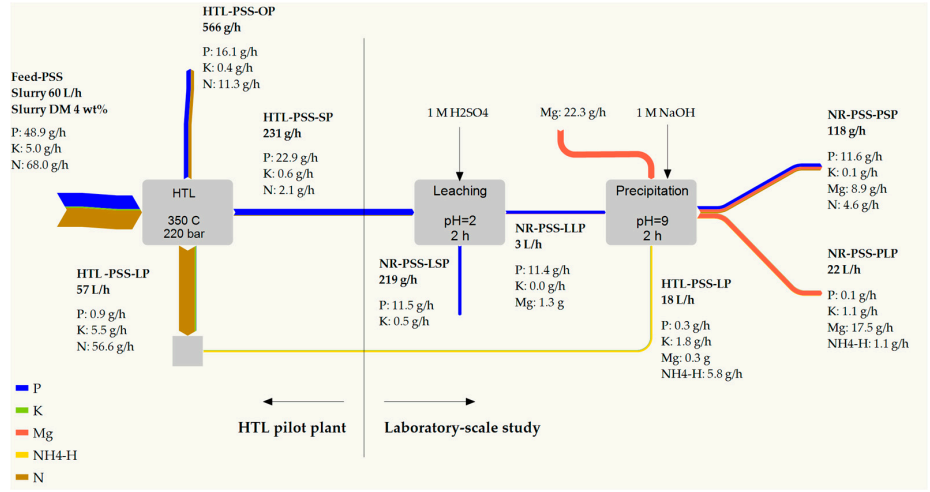

(**a**)

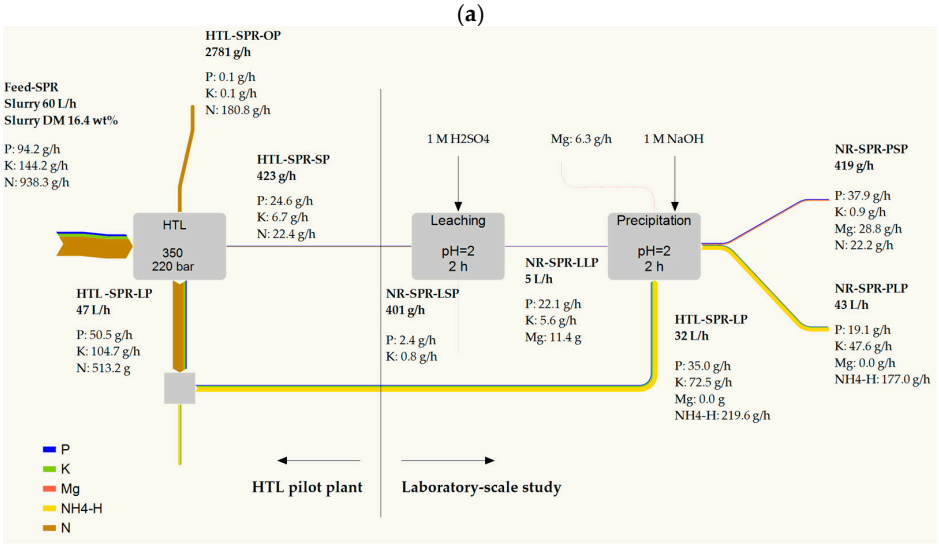

(**b**)

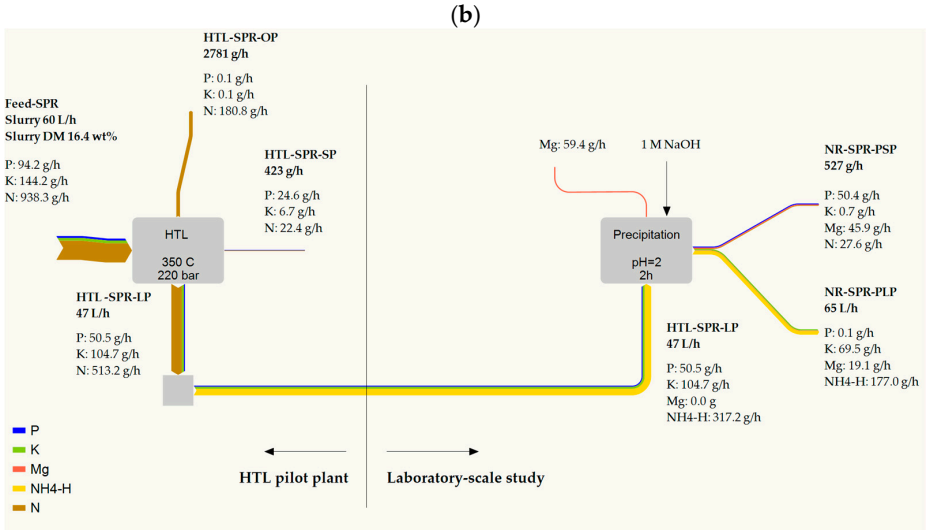

(**c**)

Figure 6. Overall process considerations and mass flow of macronutrients for HTL of PSS (**a**) and *SPR* (**b**,**c**). The sample ID can be found in Figure 1.

Figure 6b,c presents macronutrients flow from *SPR* in the precipitation struvite from the mix solution of leachate and the HTL liquid phase and in the direct precipitation from the HTL liquid phase.

Approximately 40% and 54% of the phosphate from the unprocessed *SPR* was recovered in the struvite in Figure 6b,c, respectively. The HTL liquid phase from *SPR* is the ammonium-rich stream, and an excess of ammonium ions presents in both cases, which can cause a low recovery rate of ammonium ions. In the first case, the amount of ammonium that is required for struvite precipitation can be regulated and optimized by adjusting the mix ratio of leachate and the HTL liquid phase. Meanwhile, in the case of direct precipitation, it is more difficult to control and adjust the optimal NH_4^+:PO_4^{3-}. Further research should consider how to approach the ammonium-rich post-precipitation liquid phase. Possible strategies include stripping ammonia and recovering it in the form of the fertilizer ammonium sulfate [89] or using activated carbon as a sorbent for ammonium separation. In such a case, the struvite crystallization could be beneficial as a pre-treatment technique.

In summary, the recovery of phosphate from the HTL residual stream was successfully performed. The process variations (H_2SO_4, NaOH, and Mg dosages as well as the amount of the HTL liquid phase) and the composition of the initial solution are the main challenges in developing an efficient and cost-effective process design for the struvite precipitation.

4. Conclusions

Biorefineries that are based on HTL and utilize feedstocks with high nutrient loads can add value to the production chain of liquid biofuels relatively easily through the addition of struvite-producing units. For high-protein and low-ash feedstock, such as *SPR*, a one-step approach to directly precipitate struvite from the HTL liquid phase recovers most of the phosphate. Still, ammonium is present in such substantial loads that additional treatment becomes mandatory. Since ammonia stripping is usually a disadvantage of struvite precipitation, such effect might be forced tothe extent that ammonia is recovered as, for example, ammonia sulfate during the production of struvite. The sewage sludge that is processed by HTL provides a solid residue that is suitable for recovering phosphate as struvite by means of acid leaching and the addition of released phosphate to the ammonium-rich HTL liquid phase. The larger problem in recovering phosphate is to recover the fine particulate solid residue that is dispersed in the bio-crude oil. Further development of possible in-line filtration during HTL might resolve this problem and enable, along with a future optimization study of precipitation and leaching step, a way to higher phosphate recovery rates for the HTL solid residue, as illustrated by the mass flow.

Supplementary Materials: The following are available online at http://www.mdpi.com/1996-1073/13/2/379/s1, As supplementary materials are available: Figure S1. The particle-size distribution in HTL oil phase from PSS; Figure S2. XRD analysis of HTL solid phase from PSS and *SPR*; and Figure S3. XRD analysis of precipitate from PSS and *SPR*.

Author Contributions: Conceptualization: E.O., G.C.B.; analysis and investigation: E.O.; data analyses: E.O., G.C.B.; writing and preparation of manuscript: E.O., G.C.B., A.K.; funding acquisition: G.C.B. All authors have read and agreed to the published version of the manuscript.

Funding: This research was funded by the European Union's Horizon 2020 research and innovation program under grant agreement No 764734 (HyFlexFuel-Hydrothermal liquefaction: Enhanced performance and feedstock flexibility for efficient biofuel production).

Acknowledgments: We gratefully thank the Department of Engineering at Aarhus University (Patrick Biller and Konstantinos Anastasakis) for providing samples for investigation. We are grateful to Michael Zimmermann (Karlsruhe Institute of Technology (KIT)) for XRD and SEM analyses.

Conflicts of Interest: The authors declare no conflict of interest.

References

1. Jong, S.D.; Hoefnagels, R.; Faaij, A.; Slade, R.; Mawhood, R.; Junginger, M. The feasibility of short-term production strategies for renewable jet fuels—A comprehensive techno-economic comparison. *Biofuels Bioprod. Bioref.* **2015**, *9*, 778–800. [CrossRef]
2. Biller, P.; Roth, A. Hydrothermal Liquefaction: A Promising Pathway Towards Renewable Jet Fuel. In *Biokerosene: Status and Prospects*; Kaltschmitt, M., Neuling, U., Eds.; Springer: Berlin/Heidelberg, Germany, 2018; pp. 607–635. ISBN 978-3-662-53065-8.
3. Peterson, A.A.; Vogel, F.; Lachance, R.P.; Fröling, M.; Michael, J.; Antal, J.R.; Tester, J.W. Thermochemical biofuel production in hydrothermal media: A review of sub- and supercritical water technologies. *Energy Environ. Sci.* **2008**, *1*, 32–65. [CrossRef]
4. Savage, P.E.; Levine, R.B.; Huelsman, C.M. Hydrothermal Processing of Biomass. In *Thermochemical Conversion of Biomass to Liquid Fuels and Chemicals*; Crocker, M., Ed.; RSC Publishing: Cambridge, UK, 2010; Chapter 8; pp. 192–221. ISBN 978-1-84973-035-8.
5. Castello, D.; Haider, M.S.; Rosendahl, L. Catalytic upgrading of hydrothermal liquefaction biocrudes: Different challenges for different feedstocks. *Renew. Energy* **2019**, *141*, 420–430. [CrossRef]
6. Ekpo, U.; Ross, A.B.; Camargo-Valero, M.A.; Williams, P.T. A comparison of product yields and inorganic content in process streams following thermal hydrolysis and hydrothermal processing of microalgae, manure and digestate. *Bioresour. Technol.* **2016**, *200*, 951–960. [CrossRef] [PubMed]
7. Elliott, D.C.; Biller, P.; Ross, A.B.; Schmidt, A.J.; Jones, S.B. Hydrothermal liquefaction of biomass: Developments from batch to continuous process. *Bioresour. Technol.* **2015**, *178*, 147–156. [CrossRef] [PubMed]
8. Elliott, D.C. Review of recent reports on process technology for thermochemical conversion of whole algae to liquid fuels. *Algal Res.* **2016**, *13*, 255–263. [CrossRef]
9. López Barreiro, D.; Prins, W.; Ronsse, F.; Brilman, W. Hydrothermal liquefaction (HTL) of microalgae for biofuel production: State of the art review and future prospects. *Biomass Bioenergy* **2013**, *53*, 113–127. [CrossRef]
10. Castello, D.; Pedersen, T.; Rosendahl, L. Continuous Hydrothermal Liquefaction of Biomass: A Critical Review. *Energies* **2018**, *11*, 3165. [CrossRef]
11. Edmundson, S.; Huesemann, M.; Kruk, R.; Lemmon, T.; Billing, J.; Schmidt, A.; Anderson, D. Phosphorus and nitrogen recycle following algal bio-crude production via continuous hydrothermal liquefaction. *Algal Res.* **2017**, *26*, 415–421. [CrossRef]
12. McGinn, P.J.; Park, K.C.; Robertson, G.; Scoles, L.; Ma, W.; Singh, D. Strategies for recovery and recycling of nutrients from municipal sewage treatment effluent and hydrothermal liquefaction wastewaters for the growth of the microalga Scenedesmus sp. AMDD. *Algal Res.* **2019**, *38*, 101418. [CrossRef]
13. Suzuki, A.; Nakamura, T.; Yokoyama, S.-Y.; Ogi, T.; Koguchi, K. Conversion of sewage sludge to heavy oil by direct thermochemical liquefaction. *J. Chem. Eng. Jpn. JCEJ* **1988**, *21*, 288–293. [CrossRef]
14. Vardon, D.R.; Sharma, B.K.; Scott, J.; Yu, G.; Wang, Z.; Schideman, L.; Zhang, Y.; Strathmann, T.J. Chemical properties of biocrude oil from the hydrothermal liquefaction of Spirulina algae, swine manure, and digested anaerobic sludge. *Bioresour. Technol.* **2011**, *102*, 8295–8303. [CrossRef] [PubMed]
15. Marrone, P.A.; Elliott, D.C.; Billing, J.M.; Hallen, R.T.; Hart, T.R.; Kadota, P.; Moeller, J.C.; Randel, M.A.; Schmidt, A.J. Bench-Scale Evaluation of Hydrothermal Processing Technology for Conversion of Wastewater Solids to Fuels. *Water Environ. Res.* **2018**, *90*, 329–342. [CrossRef] [PubMed]
16. Peccia, J.; Westerhoff, P. We Should Expect More out of Our Sewage Sludge. *Environ. Sci. Technol.* **2015**, *49*, 8271–8276. [CrossRef] [PubMed]
17. Huang, H.-J.; Yuan, X.-Z. The migration and transformation behaviors of heavy metals during the hydrothermal treatment of sewage sludge. *Bioresour. Technol.* **2016**, *200*, 991–998. [CrossRef] [PubMed]
18. Shao, J.; Yuan, X.; Leng, L.; Huang, H.; Jiang, L.; Wang, H.; Chen, X.; Zeng, G. The comparison of the migration and transformation behavior of heavy metals during pyrolysis and liquefaction of municipal sewage sludge, paper mill sludge, and slaughterhouse sludge. *Bioresour. Technol.* **2015**, *198*, 16–22. [CrossRef]
19. Becker, G.C.; Wüst, D.; Köhler, H.; Lautenbach, A.; Kruse, A. Novel approach of phosphate-reclamation as struvite from sewage sludge by utilising hydrothermal carbonization. *J. Environ. Manag.* **2019**, *238*, 119–125. [CrossRef]

20. Yu, Y.; Lei, Z.; Yuan, T.; Jiang, Y.; Chen, N.; Feng, C.; Shimizu, K.; Zhang, Z. Simultaneous phosphorus and nitrogen recovery from anaerobically digested sludge using a hybrid system coupling hydrothermal pretreatment with MAP precipitation. *Bioresour. Technol.* **2017**, *243*, 634–640. [CrossRef]
21. Zhao, X.; Becker, G.C.; Faweya, N.; Rodriguez Correa, C.; Yang, S.; Xie, X.; Kruse, A. Fertilizer and activated carbon production by hydrothermal carbonization of digestate. *Biomass Convers. Biorefin.* **2018**, *8*, 423–436. [CrossRef]
22. Zhao, X.; Stökle, K.; Becker, G.C.; Zimmermann, M.; Kruse, A. Hydrothermal carbonization of Spirulina platensis and Chlorella vulgaris combined with protein isolation and struvite production. *Bioresour. Technol. Rep.* **2019**, *6*, 159–167. [CrossRef]
23. Bauer, S.; Cheng, F.; Colosi, L. Evaluating the Impacts of ACP Management on the Energy Performance of Hydrothermal Liquefaction via Nutrient Recovery. *Energies* **2019**, *12*, 729. [CrossRef]
24. Dyhrman, S.T. Nutrients and Their Acquisition: Phosphorus Physiology in Microalgae. In *The Physiology of Microalgae*; Beardall, J., Raven, J.A., Borowitzka, M.A., Eds.; Springer: Cham, Switzerland, 2016; pp. 155–183. ISBN 978-3-319-24945-2.
25. Valdez, P.J.; Nelson, M.C.; Wang, H.Y.; Lin, X.N.; Savage, P.E. Hydrothermal liquefaction of Nannochloropsis sp.: Systematic study of process variables and analysis of the product fractions. *Biomass Bioenergy* **2012**, *46*, 317–331. [CrossRef]
26. Jena, U.; Vaidyanathan, N.; Chinnasamy, S.; Das, K.C. Evaluation of microalgae cultivation using recovered aqueous co-product from thermochemical liquefaction of algal biomass. *Bioresour. Technol.* **2011**, *102*, 3380–3387. [CrossRef] [PubMed]
27. Bagnoud-Velásquez, M.; Schmid-Staiger, U.; Peng, G.; Vogel, F.; Ludwig, C. First developments towards closing the nutrient cycle in a biofuel production process. *Algal Res.* **2015**, *8*, 76–82. [CrossRef]
28. Barbera, E.; Bertucco, A.; Kumar, S. Nutrients recovery and recycling in algae processing for biofuels production. *Renew. Sustain. Energy Rev.* **2018**, *90*, 28–42. [CrossRef]
29. López Barreiro, D.; Bauer, M.; Hornung, U.; Posten, C.; Kruse, A.; Prins, W. Cultivation of microalgae with recovered nutrients after hydrothermal liquefaction. *Algal Res.* **2015**, *9*, 99–106. [CrossRef]
30. Leng, L.; Li, J.; Wen, Z.; Zhou, W. Use of microalgae to recycle nutrients in aqueous phase derived from hydrothermal liquefaction process. *Bioresour. Technol.* **2018**, *256*, 529–542. [CrossRef]
31. Gu, Y.; Zhang, X.; Deal, B.; Han, L. Biological systems for treatment and valorization of wastewater generated from hydrothermal liquefaction of biomass and systems thinking: A review. *Bioresour. Technol.* **2019**, *278*, 329–345. [CrossRef]
32. Biller, P.; Ross, A.B.; Skill, S.C.; Lea-Langton, A.; Balasundaram, B.; Hall, C.; Riley, R.; Llewellyn, C.A. Nutrient recycling of aqueous phase for microalgae cultivation from the hydrothermal liquefaction process. *Algal Res.* **2012**, *1*, 70–76. [CrossRef]
33. Garcia Alba, L.; Torri, C.; Fabbri, D.; Kersten, S.R.A.; Brilman, D.W.F. Microalgae growth on the aqueous phase from Hydrothermal Liquefaction of the same microalgae. *Chem. Eng. J.* **2013**, *228*, 214–223. [CrossRef]
34. Shanmugam, S.R.; Adhikari, S.; Shakya, R. Nutrient removal and energy production from aqueous phase of bio-oil generated via hydrothermal liquefaction of algae. *Bioresour. Technol.* **2017**, *230*, 43–48. [CrossRef] [PubMed]
35. Peng, L.; Dai, H.; Wu, Y.; Peng, Y.; Lu, X. A comprehensive review of phosphorus recovery from wastewater by crystallization processes. *Chemosphere* **2018**, *197*, 768–781. [CrossRef] [PubMed]
36. Zhang, T.; He, X.; Deng, Y.; Tsang, D.C.W.; Jiang, R.; Becker, G.C.; Kruse, A. Phosphorus recovered from digestate by hydrothermal processes with struvite crystallization and its potential as a fertilizer. *Sci. Total Environ.* **2019**, *698*, 134240. [CrossRef]
37. Le Corre, K.S.; Valsami-Jones, E.; Hobbs, P.; Parsons, S.A. Phosphorus Recovery from Wastewater by Struvite Crystallization: A Review. *Crit. Rev. Environ. Sci. Technol.* **2009**, *39*, 433–477. [CrossRef]
38. Anastasakis, K.; Biller, P.; Madsen, R.; Glasius, M.; Johannsen, I. Continuous Hydrothermal Liquefaction of Biomass in a Novel Pilot Plant with Heat Recovery and Hydraulic Oscillation. *Energies* **2018**, *11*, 2695. [CrossRef]
39. Ruban, V.; López-Sánchez, J.F.; Pardo, P.; Rauret, G.; Muntau, H.; Quevauviller, P. Harmonized protocol and certified reference material for the determination of extractable contents of phosphorus in freshwater sediments—A synthesis of recent works. *Fresenius J. Anal. Chem.* **2001**, *370*, 224–228. [CrossRef] [PubMed]

40. González Medeiros, J.J.; Pérez Cid, B.; Fernández Gómez, E. Analytical phosphorus fractionation in sewage sludge and sediment samples. *Anal. Bioanal. Chem.* **2005**, *381*, 873–878. [CrossRef]
41. Schüller, H. Die CAL-Methode, eine neue Methode zur Bestimmung des pflanzenverfügbaren Phosphates in Böden. *Z. Pflanzenernaehr. Bodenk.* **1969**, *123*, 48–63. [CrossRef]
42. Thun, R.; Hoffmann, G. *Die Untersuchung von Böden, 4., neubearb. u. erw. Aufl*; VDLUFA-Verl.: Darmstadt, Germany, 2012; ISBN 9783941273139.
43. Ovsyannikova, E.; Arauzo, P.J.; Becker, G.C.; Kruse, A. Experimental and thermodynamic studies of phosphate behavior during the hydrothermal carbonization of sewage sludge. *Sci. Total Environ.* **2019**, *692*, 147–156. [CrossRef]
44. Jena, U.; Das, K.C.; Kastner, J.R. Effect of operating conditions of thermochemical liquefaction on biocrude production from Spirulina platensis. *Bioresour. Technol.* **2011**, *102*, 6221–6229. [CrossRef]
45. Haider, M.; Castello, D.; Michalski, K.; Pedersen, T.; Rosendahl, L. Catalytic Hydrotreatment of Microalgae Biocrude from Continuous Hydrothermal Liquefaction: Heteroatom Removal and Their Distribution in Distillation Cuts. *Energies* **2018**, *11*, 3360. [CrossRef]
46. Lemoine, F.; Maupin, I.; Lemée, L.; Lavoie, J.-M.; Lemberton, J.-L.; Pouilloux, Y.; Pinard, L. Alternative fuel production by catalytic hydroliquefaction of solid municipal wastes, primary sludges and microalgae. *Bioresour. Technol.* **2013**, *142*, 1–8. [CrossRef] [PubMed]
47. Madsen, R.B.; Glasius, M. How Do Hydrothermal Liquefaction Conditions and Feedstock Type Influence Product Distribution and Elemental Composition? *Ind. Eng. Chem. Res.* **2019**. [CrossRef]
48. Juneja, A.; Ceballos, R.; Murthy, G. Effects of Environmental Factors and Nutrient Availability on the Biochemical Composition of Algae for Biofuels Production: A Review. *Energies* **2013**, *6*, 4607–4638. [CrossRef]
49. Tabatabai, M.; Frankenberger, W. Chemical composition of sewage sludges in Iowa. *Res. Bull.* **1979**, *36*, 1.
50. Biller, P.; Ross, A.B. Potential yields and properties of oil from the hydrothermal liquefaction of microalgae with different biochemical content. *Bioresour. Technol.* **2011**, *102*, 215–225. [CrossRef]
51. Jarvis, J.M.; Sudasinghe, N.M.; Albrecht, K.O.; Schmidt, A.J.; Hallen, R.T.; Anderson, D.B.; Billing, J.M.; Schaub, T.M. Impact of iron porphyrin complexes when hydroprocessing algal HTL biocrude. *Fuel* **2016**, *182*, 411–418. [CrossRef]
52. Jensen, C.U. PIUS—Hydrofaction(TM) Platform with Integrated Upgrading Step. Ph.d.-serien for Det Ingeniør- og Naturvidenskabelige Fakultet. Ph.D. Thesis, Aalborg Universitet, Aalborg, Denmark, 2018.
53. Speight, J.G. *Handbook of Petroleum Product Analysis*, 2nd ed.; Wiley: Hoboken, NJ, USA, 2015; ISBN 9781118986370.
54. Jensen, C.U.; Rosendahl, L.A.; Olofsson, G. Impact of nitrogenous alkaline agent on continuous HTL of lignocellulosic biomass and biocrude upgrading. *Fuel Process. Technol.* **2017**, *159*, 376–385. [CrossRef]
55. Kubička, D.; Horáček, J. Deactivation of HDS catalysts in deoxygenation of vegetable oils. *Appl. Catal. A Gen.* **2011**, *394*, 9–17. [CrossRef]
56. Jiang, J.; Savage, P.E. Metals and Other Elements in Biocrude from Fast and Isothermal Hydrothermal Liquefaction of Microalgae. *Energy Fuels* **2018**, *32*, 4118–4126. [CrossRef]
57. Jiang, J.; Savage, P.E. Influence of process conditions and interventions on metals content in biocrude from hydrothermal liquefaction of microalgae. *Algal Res.* **2017**, *26*, 131–134. [CrossRef]
58. Marchetti, A.; Maldonado, M.T. Iron. In *The Physiology of Microalgae*; Beardall, J., Raven, J.A., Borowitzka, M.A., Eds.; Springer: Cham, Switzerland, 2016; pp. 233–279. ISBN 978-3-319-24945-2.
59. Jiang, J.; Savage, P.E. Using Solvents to Reduce the Metal Content in Crude Bio-oil from Hydrothermal Liquefaction of Microalgae. *Ind. Eng. Chem. Res.* **2019**. [CrossRef]
60. Agblevor, F.A.; Besler, S. Inorganic Compounds in Biomass Feedstocks. 1. Effect on the Quality of Fast Pyrolysis Oils. *Energy Fuels* **1996**, *10*, 293–298. [CrossRef]
61. Elliott, D.C.; Hart, T.R.; Schmidt, A.J.; Neuenschwander, G.G.; Rotness, L.J.; Olarte, M.V.; Zacher, A.H.; Albrecht, K.O.; Hallen, R.T.; Holladay, J.E. Process development for hydrothermal liquefaction of algae feedstocks in a continuous-flow reactor. *Algal Res.* **2013**, *2*, 445–454. [CrossRef]
62. Hable, R.D.; Alimoradi, S.; Sturm, B.S.M.; Stagg-Williams, S.M. Simultaneous solid and biocrude product transformations from the hydrothermal treatment of high pH-induced flocculated algae at varying Ca concentrations. *Algal Res.* **2019**, *40*, 101501. [CrossRef]
63. Leusbrock, I.; Metz, S.J.; Rexwinkel, G.; Versteeg, G.F. The solubilities of phosphate and sulfate salts in supercritical water. *J. Supercrit. Fluids* **2010**, *54*, 1–8. [CrossRef]

64. Roberts, G.W.; Sturm, B.S.M.; Hamdeh, U.; Stanton, G.E.; Rocha, A.; Kinsella, T.L.; Fortier, M.-O.P.; Sazdar, S.; Detamore, M.S.; Stagg-Williams, S.M. Promoting catalysis and high-value product streams by in situ hydroxyapatite crystallization during hydrothermal liquefaction of microalgae cultivated with reclaimed nutrients. *Green Chem.* **2015**, *17*, 2560–2569. [CrossRef]
65. Riman, R.E.; Suchanek, W.L.; Byrappa, K.; Chen, C.-W.; Shuk, P.; Oakes, C.S. Solution synthesis of hydroxyapatite designer particulates. *Solid State Ionics* **2002**, *151*, 393–402. [CrossRef]
66. Christensen, P.S.; Peng, G.; Vogel, F.; Iversen, B.B. Hydrothermal Liquefaction of the Microalgae Phaeodactylum tricornutum: Impact of Reaction Conditions on Product and Elemental Distribution. *Energy Fuels* **2014**, *28*, 5792–5803. [CrossRef]
67. Anastasakis, K.; Ross, A.B. Hydrothermal liquefaction of the brown macro-alga Laminaria Saccharina: Effect of reaction conditions on product distribution and composition. *Bioresour. Technol.* **2011**, *102*, 4876–4883. [CrossRef]
68. Kruse, A.; Koch, F.; Stelzl, K.; Wüst, D.; Zeller, M. Fate of Nitrogen during Hydrothermal Carbonization. *Energy Fuels* **2016**, *30*, 8037–8042. [CrossRef]
69. Biller, P.; Johannsen, I.; Dos Passos, J.S.; Ottosen, L.D.M. Primary sewage sludge filtration using biomass filter aids and subsequent hydrothermal co-liquefaction. *Water Res.* **2018**, *130*, 58–68. [CrossRef] [PubMed]
70. Huang, R.; Tang, Y. Speciation Dynamics of Phosphorus during (Hydro)Thermal Treatments of Sewage Sludge. *Environ. Sci. Technol.* **2015**, *49*, 14466–14474. [CrossRef] [PubMed]
71. Huang, R.; Fang, C.; Lu, X.; Jiang, R.; Tang, Y. Transformation of Phosphorus during (Hydro)thermal Treatments of Solid Biowastes: Reaction Mechanisms and Implications for P Reclamation and Recycling. *Environ. Sci. Technol.* **2017**, *51*, 10284–10298. [CrossRef] [PubMed]
72. Feng, Y.; Ma, K.; Yu, T.; Bai, S.; Pei, D.; Bai, T.; Zhang, Q.; Yin, L.; Hu, Y.; Chen, D. Phosphorus Transformation in Hydrothermal Pretreatment and Steam Gasification of Sewage Sludge. *Energy Fuels* **2018**, *32*, 8545–8551. [CrossRef]
73. Xu, Y.; Yang, F.; Zhang, L.; Wang, X.; Sun, Y.; Liu, Q.; Qian, G. Migration and transformation of phosphorus in municipal sludge by the hydrothermal treatment and its directional adjustment. *Waste Manag.* **2018**, *81*, 196–201. [CrossRef]
74. Huang, R.; Fang, C.; Zhang, B.; Tang, Y. Transformations of Phosphorus Speciation during (Hydro)thermal Treatments of Animal Manures. *Environ. Sci. Technol.* **2018**, *52*, 3016–3026. [CrossRef]
75. Yakaboylu, O.; Harinck, J.; Gerton Smit, K.G.; Jong, W. Supercritical water gasification of manure: A thermodynamic equilibrium modeling approach. *Biomass Bioenergy* **2013**, *59*, 253–263. [CrossRef]
76. Stumm, W.; Morgan, J.J. *Aquatic Chemistry. Chemical Equilibria and Rates in Natural Waters*, 3rd ed.; John Wiley & Sons Inc.: New York, NY, USA; Chichester, UK; Brisbane, Australia; Toronto, ON, Canada; Singapore, 1996; ISBN 9780471511854.
77. Petzet, S.; Peplinski, B.; Cornel, P. On wet chemical phosphorus recovery from sewage sludge ash by acidic or alkaline leaching and an optimized combination of both. *Water Res.* **2012**, *46*, 3769–3780. [CrossRef]
78. Heilmann, S.M.; Molde, J.S.; Timler, J.G.; Wood, B.M.; Mikula, A.L.; Vozhdayev, G.V.; Colosky, E.C.; Spokas, K.A.; Valentas, K.J. Phosphorus reclamation through hydrothermal carbonization of animal manures. *Environ. Sci. Technol.* **2014**, *48*, 10323–10329. [CrossRef]
79. Zhang, Q.; Zhao, S.; Ye, X.; Xiao, W. Effects of organic substances on struvite crystallization and recovery. *Desalin. Water Treat.* **2016**, *57*, 10924–10933. [CrossRef]
80. Donatello, S.; Tong, D.; Cheeseman, C.R. Production of technical grade phosphoric acid from incinerator sewage sludge ash (ISSA). *Waste Manag.* **2010**, *30*, 1634–1642. [CrossRef] [PubMed]
81. Franz, M. Phosphate fertilizer from sewage sludge ash (SSA). *Waste Manag.* **2008**, *28*, 1809–1818. [CrossRef] [PubMed]
82. Donatello, S. Characteristics of Incinerated Sewage Sludge Ashes: Potential for Phosphate Extraction and Re-Use as a Pozzolanic Material in Construction Products. Ph.D. Thesis, Imperial College London, London, UK, 2009.
83. Li, B.; Huang, H.M.; Boiarkina, I.; Yu, W.; Huang, Y.F.; Wang, G.Q.; Young, B.R. Phosphorus recovery through struvite crystallisation: Recent developments in the understanding of operational factors. *J. Environ. Manag.* **2019**, *248*, 109254. [CrossRef] [PubMed]
84. Liu, Y.; Kumar, S.; Kwag, J.-H.; Ra, C. Magnesium ammonium phosphate formation, recovery and its application as valuable resources: A review. *J. Chem. Technol. Biotechnol.* **2013**, *88*, 181–189. [CrossRef]

85. Pastor, L.; Mangin, D.; Barat, R.; Seco, A. A pilot-scale study of struvite precipitation in a stirred tank reactor: Conditions influencing the process. *Bioresour. Technol.* **2008**, *99*, 6285–6291. [CrossRef]
86. Stratful, I.; Scrimshaw, M.D.; Lester, J.N. Conditions influencing the precipitation of magnesium ammonium phosphate. *Water Res.* **2001**, *35*, 4191–4199. [CrossRef]
87. Li, B.; Boiarkina, I.; Yu, W.; Huang, H.M.; Munir, T.; Wang, G.Q.; Young, B.R. Phosphorous recovery through struvite crystallization: Challenges for future design. *Sci. Total Environ.* **2019**, *648*, 1244–1256. [CrossRef]
88. Jaffer, Y.; Clark, T.A.; Pearce, P.; Parsons, S.A. Potential phosphorus recovery by struvite formation. *Water Res.* **2002**, *36*, 1834–1842. [CrossRef]
89. Ghyselbrecht, K.; Monballiu, A.; Somers, M.H.; Sigurnjak, I.; Meers, E.; Appels, L.; Meesschaert, B. Stripping and scrubbing of ammonium using common fractionating columns to prove ammonium inhibition during anaerobic digestion. *Int. J. Energy Environ. Eng.* **2018**, *9*, 447–455. [CrossRef]